A cyclic electrochemical strategy to produce acetylene from CO_2, CH_4, or alternative carbon sources†

Joshua M. McEnaney, ‡[a] Brian A. Rohr, ‡[a] Adam C. Nielander, [a] Aayush R. Singh,[a] Laurie A. King, [a] Jens K. Nørskov*[abc] and Thomas F. Jaramillo *[ab]

Electrochemical transformation of potent greenhouse gases such as CO_2 and CH_4 to produce useful carbon-based products is a highly desirable sustainability goal. However, selectivity challenges remain in aqueous electrochemical processes as selective CO_2 reduction to desired products is difficult and electrochemical CH_4 oxidation often proceeds at very low rates. The formation of C–C coupled products in these fields is particularly desirable as this provides a path for the production of high-value fuels and chemicals. We have developed a cyclic electrochemical strategy which can produce acetylene, a C–C coupled product, from such carbon sources and water, with favorable current density and selectivity. This strategy is exemplified with a lithium-mediated cycle: an active Li^0 surface is electrochemically generated from LiOH, the newly formed Li^0 reacts with a carbon source to form Li_2C_2, and Li_2C_2 is hydrolyzed to form acetylene and regenerate LiOH. We demonstrate this process primarily using CO_2 gas, achieving a current efficiency of 15% to acetylene (which represents 82% of the maximum based on stoichiometric production of oxygenated byproducts, *e.g.* $LiCO_3$ and/or Li_2O), as verified by gas chromatography and Fourier transform infrared radiation studies. We also explore CH_4, CO, and C as alternative precursors in the acetylene synthesis. Notably, the use of graphitic carbon at higher temperatures resulted in over 55% current efficiency to acetylene, with opportunity for further optimization. Importantly, this cycling method avoids the formation of common side products observed during aqueous electrochemical CO_2 and CH_4 redox reactions, such as H_2, CO, HCO_2^-, or CO_2. Theoretical considerations elucidate the feasibility and general applicability of this cycle and the process steps have been characterized with specific electrochemical and materials chemistry techniques. The continued development of this strategy may lead to a viable route for the sustainable production of C–C coupled carbon fuels and chemicals.

Introduction

Carbon dioxide and methane are two major emitted chemicals with global impact as greenhouse gases. The limited chemical versatility and limited demand *vs.* a massive supply for these gases also makes them inexpensive materials. Thus, these gasses are targeted as precursors for chemical processing to produce higher value, more useful products. Aqueous electrochemical CO_2 reduction or CH_4 oxidation are attractive routes toward sustainably converting these chemicals into higher value chemicals and fuels. However, under such aqueous conditions, CO_2 reduction is often dominated by the hydrogen evolution reaction (HER), motivating research into non-aqueous routes.[1–3] On the other hand, CH_4 is difficult to selectively oxidize on surfaces and often fully oxidizes to CO_2, if it reacts at all.[4] In order to form higher value chemical products such as $C2^+$ alcohols and long chain hydrocarbons, however, C–C coupling capability is necessary, thus this is a key challenge in electrochemical production processes.[5,6] For CO_2 electrochemical reduction, some progress has been made on copper based catalysts, one of very few systems capable of demonstrating C–C coupling and promoting selectivity to a range of higher value products.[5–9] With very few electrochemical routes to form C–C coupled products from these sources, new directions to the formation of many higher value fuels and chemicals are highly desirable.

Acetylene, as a triple bonded, C–C coupled chemical and fuel, is an important product with exceptionally diverse chemistry that can serve as a chemical precursor to polymers, fuels, coatings,

[a]*SUNCAT Center for Interface Science and Catalysis, Department of Chemical Engineering Stanford University, Shriram Center, 443 Via Ortega, Stanford, CA 94305, USA. E-mail: jaramillo@stanford.edu*

[b]*SUNCAT Center for Interface Science and Catalysis, SLAC National Accelerator Laboratory, 2575 Sand Hill Road, Menlo Park, CA 94025, USA*

[c]*Department of Physics, Technical University of Denmark, DK-2800 Kongens Lyngby, Denmark*

† Electronic supplementary information (ESI) available. See DOI: 10.1039/c9se00799g

‡ These authors contributed equally to this manuscript.

solvents, adhesives, and other carbon-based products.[10] An elegant approach to low-carbon footprint chemical processes would be to produce acetylene as a platform chemical, employing renewable electricity and atmospheric greenhouse gasses (GHGs), *e.g.* CO_2 and CH_4, as the feedstocks. In fact, long ago, acetylene was used to produce a broad range of carbon-based chemicals before the advent of fossil fuel refinery technologies. The acetylene itself was traditionally produced by thermally combining calcium oxides with carbon but required very high temperatures (~2200 °C) to form calcium carbide as an acetylene precursor. Nowadays, acetylene is primarily produced by partial methane combustion.[10,11] There is an opportunity to develop pathways to acetylene production in a low carbon-footprint manner.

We have developed a lithium-mediated electrochemical cycling strategy as an alternative pathway for the production of acetylene from H_2O and a variety of low-cost carbon feedstocks including CO_2 and CH_4. Similar to our previous work in which we produced NH_3 from N_2 and H_2O (achieving ~90% current efficiency),[12] the lithium-mediated production process comprises three distinct steps: (1) electrochemical reactive surface preparation, (2) carbon reactant activation, and (3) hydrolysis to synthesize acetylene. These steps can be cycled for continuous acetylene production (Fig. 1). Herein, we primarily focus on CO_2 reduction to acetylene *via* lithium carbidation as a baseline for this strategy. This electrochemical strategy circumvents the HER for CO_2 reduction, and for CH_4 oxidation, prevents the complete oxidation to CO_2 while still using water as a proton source. As one of very few electrochemical routes to producing C–C coupled products, this strategy represents an important direction for carbon material electrochemical synthesis with opportunities for improved efficiency.

Results

The cyclic electrochemical strategy for acetylene synthesis is conceptually outlined in Fig. 1. The three reaction steps shown in the figure are generalized as follows:

Step 1: LiOH electrolysis:

$$\text{Total cell: } 2\text{LiOH} \rightarrow 2\text{Li} + \text{H}_2\text{O} + \tfrac{1}{2}\text{O}_{2(g)}$$

$$\text{Cathode: } 2\text{Li}^+ + 2\text{e}^- \rightarrow 2\text{Li}$$

$$\text{Anode: } 2\text{OH}^- \rightarrow \text{H}_2\text{O} + \tfrac{1}{2}\text{O}_{2(g)} + 2\text{e}^-$$

Step 2: direct reaction of metallic Li with CO_2 to form Li_2C_2:

$$2\text{Li} + 2\text{CO}_2 \rightarrow \text{Li}_2\text{C}_{2(S)} + \text{X} \text{ [see Table 1]}$$

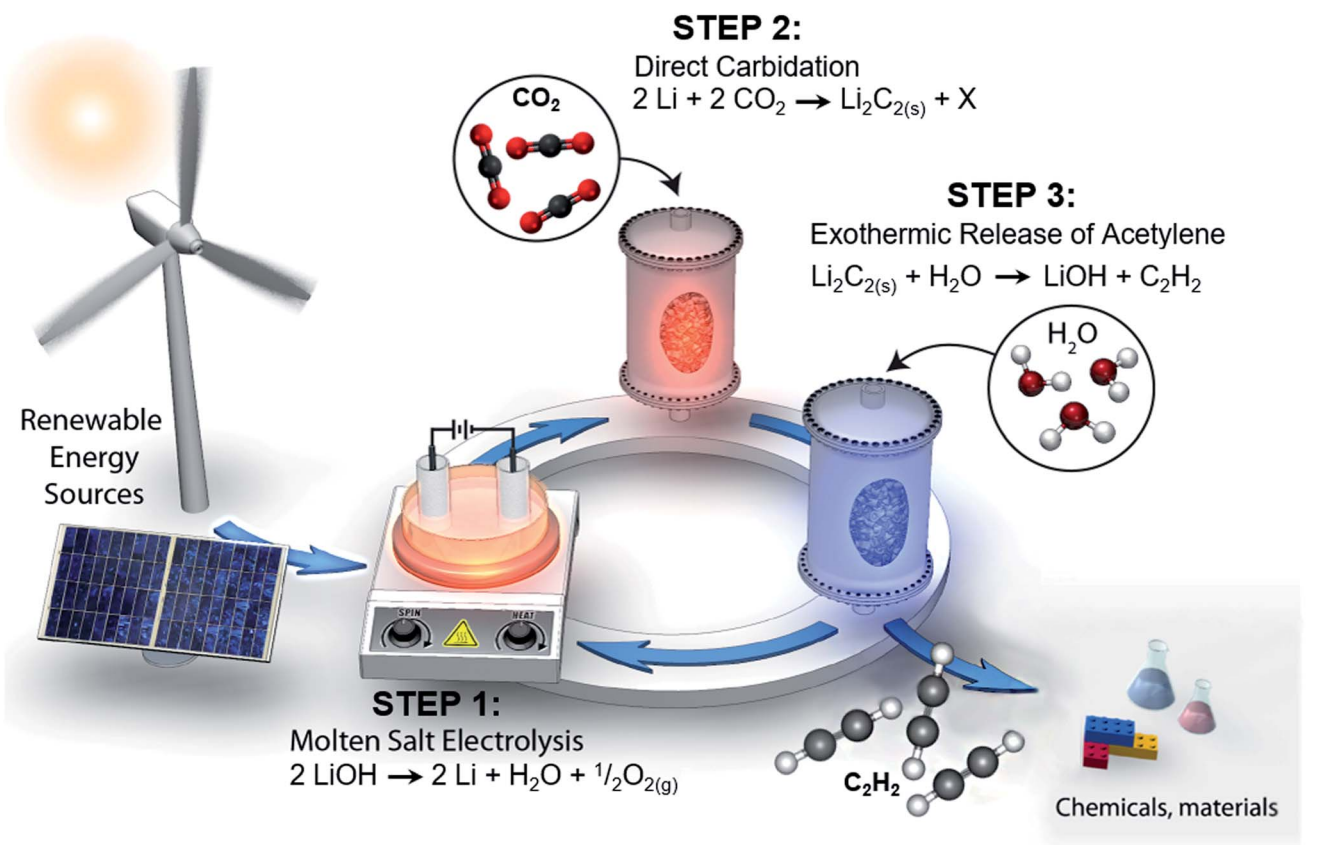

Fig. 1 Electrochemical concept cycle for acetylene production. Parallel concept cycles exist for other carbon sources such as CH_4, CO, and C for this strategy. This figure is adapted from ref. 11 with permission from the Royal Society of Chemistry.[12]

Table 1 List of possible carbon feedstocks, corresponding reasonable reaction mechanisms of these feedstocks with Li metal to produce Li_2C_2 and subsequent acetylene, and the resulting stoichiometric expectations for the ratio of Li atoms that go toward acetylene production

Feedstock	Reasonable mechanisms	$Li_{(C_2H_2)}$: $Li_{(total)}$ ratio
CO_2	$6CO_2 + 10Li \rightarrow Li_2C_2 + 4Li_2CO_3$	1 : 5
	$2CO_2 + 10Li \rightarrow Li_2C_2 + 4Li_2O$	1 : 5
CH_4	$2CH_4 + 6Li \rightarrow Li_2C_2 + 4LiH$	1 : 3
CO	$3CO + 4Li \rightarrow Li_2C_2 + Li_2CO_3$	1 : 2
	$2CO + 6Li \rightarrow Li_2C_2 + 2Li_2O$	1 : 3
C	$2C + 2Li \rightarrow Li_2C_2$	1 : 1

Step 3: hydrolytic release of C_2H_2 by reaction with H_2O

$$Li_2C_{2(s)} \rightarrow 2LiOH + C_2H_{2(g)}$$

The electrochemical nature of the metal electrolysis step, which is likely the major energy input in this reaction with the remaining reactions thermodynamically downhill, allows the cycle to be coupled directly to sustainable electricity sources.

We have experimentally demonstrated the Li-based electrochemical cycle to produce acetylene using CO_2. The first step of this electrochemical cycle was reported and discussed in our previous work on electrochemical ammonia synthesis.[12] Briefly, an LiCl–KCl/LiOH–LiCl (catholyte/anolyte) molten salt system held at 450 °C was used to produce Li metal at the cathode, and O_2 and H_2O at the anode from LiOH. A constant current (~ -0.5 A cm^{-2}) was applied for several hours to generate significant molten Li product. The electrolytically produced Li was allowed to cool, then Li was cut and pressed with steel into a thin (1 mm) pellet or slab and exposed to a flowing CO_2 atmosphere while being held at temperatures between 22 and 450 °C (Step 2). We tested the conversion efficiency of Li to C_2H_2 by adding the product of the Li + CO_2 reaction to H_2O, which rapidly hydrolyzed the solid product (Step 3). Li to C_2H_2 yields are shown in Fig. 2A for the various temperature and conditions applied. We observed small yields of acetylene product after Li carbidation at 250 °C and acetylene yields increased with increasing carbidation temperature up to 350 °C (Fig. 2A). Increasing carbidation reaction time from 4 h to 8 h at 350 °C, resulted in an increase in acetylene yields (from ~4% to ~16%). Increasing temperature beyond 400 °C resulted in a black product which did not react with water. The bulk composition of the Li + CO_2 products were examined by X-ray diffraction (XRD) (Fig. 2B). The low temperature representative Li + CO_2 product treated at 200 °C, appeared nearly unreacted and gave only a signal for Li metal with preferred orientation for the (110) peak. A moderate temperature (350 °C) representative sample was dark grey in color and non-lustrous, yielding broad peaks for Li_2O, and surprisingly no peaks for Li_2C_2. We assume the Li–C regions of the product must be amorphous to yield the significant amount of acetylene observed. The higher temperature (450 °C) representative sample shows Li_2O peaks with greater intensity as well as the formation of $LiCO_3$.

To confirm the presence of C≡C, as would be expected in the Li_2C_2 structure, Raman spectroscopy was used on a moderate temperature (350 °C, 8 h), CO_2 treated Li sample, showing a characteristic peak at 1873 cm^{-1} for the bonding feature in this structure.[13,14] This indicates the presence of the desired product (Li_2C_2) despite the lack of bulk organization to produce a prominent Li_2C_2 XRD signal (Fig. 2C). Two regions are shown, highlighting the non-uniformity of the sample. In region 1, a broad peak stretches to lower wavenumbers, which has been observed previously in amorphous Li_2C_2 samples.[14] In region 2, a small but clear peak is observed at 1873 cm^{-1}, in line with the control. The Li_2C_2 control sample was produced based on a reported procedure[15] using a Li metal and graphitic carbon powder mixture heated to 350 °C for 4 h then to 700 °C for 4 h under Ar.

To detect and quantify the acetylene product, two complementary methods were employed. Gas chromatography (GC) was used to quantify our yields against a calibration curve made from serial dilutions of 1000 ppm and 100 ppm C_2H_2 gas standards. To verify acetylene production, with a chemically specific signal gas phase Fourier Transform Infrared Spectroscopy (FTIR) was used. A representative spectrum of the gas product is shown in Fig. 2D (green) *versus* an acetylene standard gas (blue) and a HITRAN database calculated acetylene FTIR spectrum (red).

The Pourbaix diagram and overlaid cycle process steps (Fig. 3) shows that lithium carbide, the desired species to for acetylene, is not the most stable species at any applied potential. Under reducing conditions, the hydride is by far the most stable species, and under oxidizing conditions, the carbonate is by far the most stable species. This agrees well with the observed formation of $LiCO_3$ at high temperatures as a dominant thermodynamic product. We are, however, able to create a reasonable amount of the carbide, by only allowing the system to access certain species on the Pourbaix diagram during different steps of the cycle by controlling which elements are present at each step of the cycle. In the first step, plating lithium ions to form lithium metal at −4 V *vs.* SHE, the most stable species is lithium hydride, but no hydrogen is available at the cathode, thus lithium metal is formed with high selectivity. In the second step, the resulting hydride is exposed to carbon dioxide gas under no applied potential. Fig. S1† shows a Pourbaix diagram containing only the species accessible in this step of the reaction. Lithium carbonate is by far the most stable species in this step, however, the only oxygen present in the system is the oxygen in carbon dioxide gas. Therefore, while a substantial amount of carbonate is produced, any excess carbon is free to react with any excess lithium, and since this is a favorable reaction, we are able to produce a reasonable amount of lithium carbide (Table 1). Additionally, density functional theory (DFT) calculations show that the barrier for the formation of the carbide in bulk Li is much lower than the barrier for the formation of the carbonate in bulk (Fig. S2†). This agrees well with the observed data. At low temperatures, Li does not react quickly with the CO_2 at all, indicating that all barriers are too high to be quickly surmounted at low temperature. At high temperature, when the reaction is under

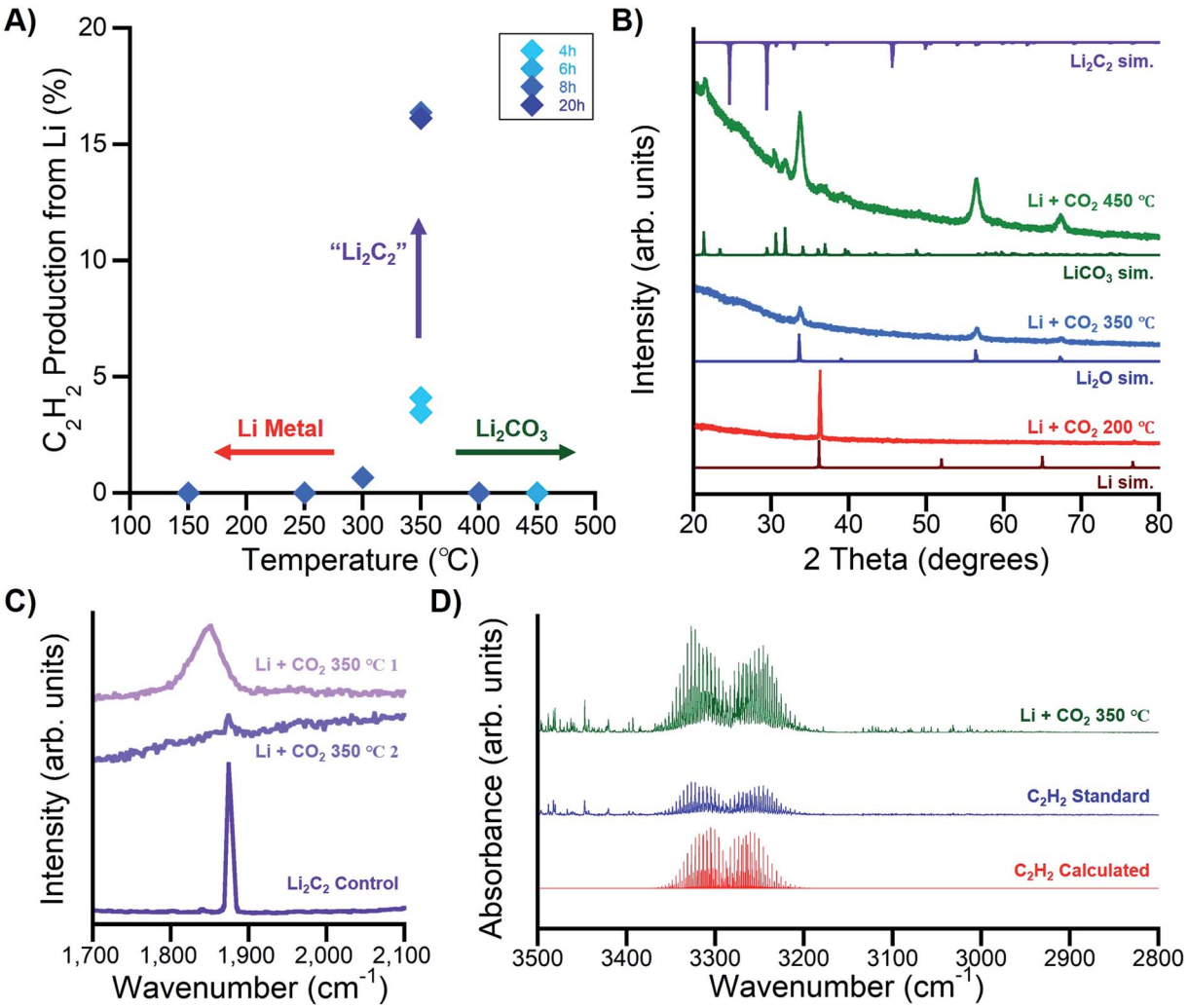

Fig. 2 (A) Acetylene yield percent based on the mols of Li used, obtained from Li carbidation from CO_2 under indicated reaction temperatures and times. (B) Representative XRD data for the experimentally synthesized Li + CO_2 products at given temperatures with relevant simulated (sim.) spectra overlaid. (C) Raman spectra, collected with an excitation laser at 432 nm, showing the characteristic peak[13,14] at 1873 cm^{-1} for Li_2C_2 on two different surface regions of a 350 °C treated sample as well as for a Li_2C_2 synthesized control. (D) Representative FTIR signal for Li–C hydrolysis product sample with an acetylene standard and a HITRAN calculated acetylene spectra[16] for reference.

thermodynamic control, $LiCO_3$ is the dominant product. At intermediate temperatures, some Li_2C_2 is formed. In the final step, water is added, providing the system with access to the Li^+ line on the Pourbaix diagram, which is very stable at 0 V *vs.* SHE. In this final step of the cycle, water spontaneously reacts with the slab, converting the carbide and oxide lithium species to Li^+ and OH^- ions, and the cycle is complete. Future work may aim to minimize the amount of carbonate formed in the reaction or increase its solubility in the electrolyte of step 1 to promote the cycle despite this thermodynamic sink.

To improve the yields of this process, there are several strategies to look to in future studies. For example, the ratio of carbon to other elements and type of elements is likely to be important. By using CO, rather than CO_2, one may limit the amount of $LiCO_3$ and Li_2O side products, increasing the Li–C formation and thus C_2H_2 product yield. This is evident by the reaction equations shown below as the relative amount of Li required per acetylene produced changes drastically depending on the side product made and the carbon source used:

In the first reaction feedstock case, using CO_2 and forming Li_2CO_3 or Li_2O as biproducts, only 1 in 5 reduced Li metal atoms is directly used for making acetylene (Table 1). Considering this, we are approaching the hypothetical maximum yield from CO_2 of 20% unless the oxygen atoms can be creatively scavenged (16.4% Li conversion to acetylene represents 82% of the maximum based on the stoichiometry presented in Table 1). By using CH_4 we change the byproduct to LiH, which will hydrolyze to form hydrogen and reform LiOH. Methane as a carbon source increases the ratio to 1 in 3 Li metal atoms toward making acetylene. In the third case, CO as a carbon source allows up to 1 in 2 Li metal atoms toward C_2H_2 (for an $LiCO_3$ byproduct, 1 in 3 if Li_2O is the byproduct). The ideal case for efficiency, the final reaction mechanism of Table 1, is a process to convert Li metal and carbon directly into Li_2C_2, where 1 in 1 Li metal atoms

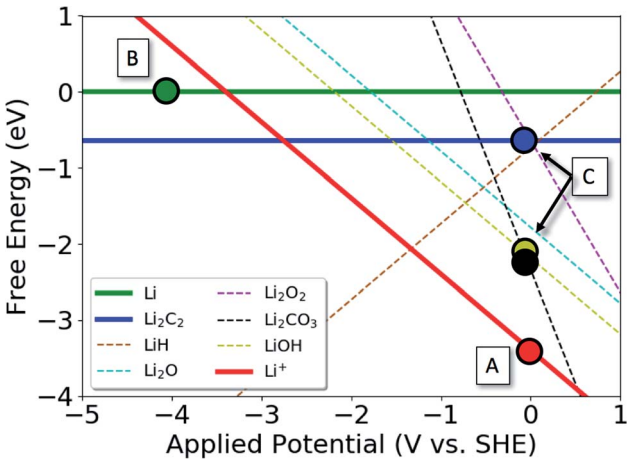

Fig. 3 Phase diagram showing the relative thermodynamic behavior of Li–C–O–H species as well as the cyclic process for electrochemical production of acetylene. In this figure, steps 1, 2, and 3 of our process are A → B, B → C, and C → A, respectively. State A is lithium ions at 0 V *vs.* SHE. State B is lithium metal, which is produced by changing the applied potential to −4 V *vs.* SHE, and state C is a mixture of Li–C–O products, obtained by exposing Li to CO_2.

could be used toward acetylene, however, carbon itself is typically a significantly more expensive reagent, resulting in a tradeoff. Each of these cases assumes that one is not losing gas in the form of O_2, CO, or H_2 (from CH_4), nor forming solid carbon instead of the indicated products, which may occur to some extent on the Li reagent. Probing the reaction dynamics of product formation here will be important for further studies. We performed several preliminary tests using CH_4, CO, and C reagents. Each also successfully yielded acetylene, however, CH_4 can result in carbon coking of the Li surface, preventing further reaction, and limiting yields to ~3% so far (see Fig. S3 in the ESI†). This seemingly low yield from Li results in an over 2% current efficiency to acetylene. However, considering that aqueous electrochemical methane oxidation typically operate at low current densities (<1 mA cm^{-2}) for primarily CO_2 and CO production, this alternative method implores further study.[17] Solid oxide fuel cell methane dehydrogenation cells can produce some C_2 products but require significantly higher operating temperatures (~700–1000 °C).[17] Next, an initial attempt at using a 10% CO in argon source, at a temperature or 350 °C and time of 8 h resulted in an ~11% acetylene yield from Li. Finally, by using a graphitic carbon reagent we were able to observe 66% acetylene production from Li (or 58% current efficiency, using the same 700 °C high temperature treatment as in the Raman control sample). It is likely that the CH_4, CO, and C results can be significantly improved with further study and optimization.

One can imagine a number of future opportunities to improve yield. For example, by continuing to hold the Li product under a negative potential while applying the carbon source. The pourbaix diagram (Fig. 3) indicates that at −4 V, Li_2C_2 becomes the thermodynamically favored product over Li_2O or $LiCO_3$. In the case of CH_4, however, the LiH becomes more thermodynamically favored with more negative potential, which may limit efficiency. Interestingly, intentional formation of LiH may be beneficial as LiH is reported to react directly with C at a low temperature of only 400–500 °C (rather than the 700 °C reaction of C with Li in this paper) to form Li_2C_2 and C_2H_2.[18] One may also improve yield if one can prevent coking, surface coating, or byproduct formation which may be possible with the addition of specific defects into the Li lattice, or possibly by seeding the Li with Li_2C_2 crystals to promote the formation of Li–C. Finally, lithium is not uniquely capable of these carbidation and hydrolysis reactions, and other metal carbides may be formed with larger windows of temperature and reactant opportunity to be selective for acetylene yield. Calcium, for example, is an obvious candidate for electrochemical cycling as calcium carbide was the basis for acetylene synthesis before fossil fuels became the primary source.[10]

Conclusions

In summary, we have introduced and demonstrated a unique approach for electrochemical production of C–C coupled acetylene using CO_2 and H_2O at atmospheric pressure. This was enabled by a lithium mediated cycling process and resulted in ~15% current efficiency to acetylene, based on Li produced and used (which represents 82% of the maximum based on stoichiometric production of oxygenated byproducts, *e.g.* $LiCO_3$ and/or Li_2O). We have also outlined the generalization of this method to use CH_4, CO, or other sources of carbon with opportunity for even greater selectivity to acetylene based on reactant stoichiometries and an understanding of the corresponding Pourbaix diagram. Preliminary testing with graphitic carbon as the carbon source increased current efficiency to over 55%. This electrochemical C–C coupling process can circumvent the competing HER reaction of typical water-based electrocatalysis, by physically and temporally separating the electrochemical activation and protonation steps of the acetylene synthesis, though it does have selectivity issues to overcome in the form of undesirable lithium side products. If the selectivity of this production process can be further improved, it may lead to a potentially sustainable source of acetylene, which is an excellent precursor to many of the chemicals that fossil fuels provide for us today.

Experimental

Chemicals and materials

Lithium hydroxide [≥98%, LiOH, powder, Sigma-Aldrich], lithium chloride [≥99%, LiCl, anhydrous powder, Sigma-Aldrich], potassium chloride [≥99%, KCl, anhydrous powder, Sigma-Aldrich], stainless steel foil [Fe : Cr : Ni; 70 : 19 : 11 wt%, 0.5 mm thick, Alfa Aesar], graphite rod, nickel rod, carbon dioxide [≥99.999%, CO_2, gas, airgas], methane [≥99.999%, CH_4, gas, Praxair], DI Millipore water, porous alumina diffusion barrier tube [80 mm height × 27 mm outer diameter (OD) × 3 mm thickness, P-3-C material, 1.7 mm average pore diameter, single closed end tube, CoorsTek], alumina round dish [35 mL, 25 mm height × 50 mm OD × 3 mm thick, AdValue Technology], cylindrical alumina crucible [5 mL, 26 mm height × 20 mm OD × 1 mm thick, 2 mm diameter side wall hole, AdValue Technology].

Electrolysis of LiOH

The first step of the electrochemical process was executed as described previously in our work on electrochemical ammonia synthesis.[12] (See Fig. S4 in the ESI† for additional electrochemical characterization.) Note: lithium reacts violently with water and hot molten salts can be hazardous, thus only appropriately trained personnel with proper safety precautions and PPE should attempt these reactions. An aluminum oxide cylindrical crucible was used as the major cell container. This crucible was equipped with a steel foil cathode and graphite rod anode for electrolysis reactions. A small porous alumina container surrounded the anode to preventing undesirable side reactions by isolating the anodic and cathodic reactants and products. Li was produced by LiOH electrolysis in this cell by applying a constant current (-0.5 A) over a 1–4 h time period. Li product was collected in a solid alumina cylindrical crucible surrounding the cathode, with a small 2 mm hole bored out to maintain electrical contact. Further electrochemical characterization, product characterization, and experimental notes can be found in our previous work.

Li–C synthesis from Li and CO_2, CH_4, or C

Li was produced in excess from LiOH electrolysis and collected from the small crucible containing the steel working electrode and the molten salt mixture. The melt was transferred to a steel crucible and allowed to cool. Li metal was brought above its melting temperature (180 °C) to isolate it from solid salts of the electrolyte, and the liquid product was decanted into a second steel crucible. Solid, cooled Li was cut and pressed between steel into ~1 mm thick pellets. The mass of these Li pellets was measured (approx. 0.01 g each) and the pellets were transferred from the Ar glovebox in a septum capped vial to a CO_2 or CH_4 purged tube furnace. Li was very briefly (15 s) exposed to air where the surface would slightly tarnish during transfer. Heat was applied under the carbonated gas flow for the desired duration (0–500 °C, 0–20 hours). Resulting gray to black pellets were collected in scintillation vials and stored in the Ar glovebox briefly until hydrolysis testing. For use of C instead of a gas reactant, graphitic carbon powder was added to solid Li in a steel crucible in the Ar-filled glovebox, using a 2 : 1 C to Li ratio. The Li + graphitic carbon was pressed into a pellet in the glovebox as above. In this case, Ar was used as the carrier gas in the tube furnace for step 2, to keep an inert atmosphere during this reaction, which was held at 350 °C for 4 hours then at 700 °C for 4 hours.

Acetylene synthesis from Li–C and H_2O

For the acetylene synthesis step, we hydrolyzed our Li–C samples using the following procedure. The Li–C pellet was removed from the glovebox in an 8 mL, capped glass vial. An inverted graduated cylinder was equipped with a septum capped top such that gas samples could be collected from the septum. The graduated cylinder and large beaker were filled with <Millipore pure de-ionized water> and the sample vial containing the Li–C pellet was uncapped directly into the submerged graduated cylinder. Thus, all gases evolved from the pellet sample, including the gas from the sample vial, were collected in the graduated cylinder for detection and quantification of gas species. Caution: this hydrolysis reaction is exothermic in general, and possible unreacted Li (and LiH in the CH_4 case) can rapidly evolve hydrogen gas, thus extra caution, preparation, and appropriate PPE should always be used. To demonstrate cyclability, we have dried the oxidized lithium products (hydroxide ± carbonate species) and re-dissolved them in the molten anolyte with successful continued production of Li. We note, however that the solubility of carbonate in the electrolyte is limited and could become problematic in cases where carbonate is produced.

Acetylene detection and quantification

The acetylene yield was determined by the concentration signal from a gas chromatograph (GC) with flame ionization detection (FID) and the total volume of evolved product gas, considering the average volume of non-product gas from the sample vial. The sample gas (100 μL) was injected into the GC. The sample peak was quantified against a calibration curve using 1000 ppm acetylene gas and a series of dilutions using the same septum capped graduated cylinder reaction apparatus described above. While the elution time for gas samples matched that of the acetylene standard, exact chemical signal verification was obtained using a gas phase FTIR cell. For this, the gas cell was first evacuated with the equipped house vacuum. The remaining sample gas (using up to 100 mL) was added *via* syringe directly to the gas phase FTIR cell. Resulting spectra gave clear signals for acetylene when present and were used to double check relative expected signal strength for quantity verification.

Current efficiency calculation

$$\mathrm{CE}\ (\%) = \frac{\text{coulombic equivalent of } C_2H_2 \text{ produced}}{\text{coulombic equivalent of the maximum possible } C_2H_2 \text{ that could have been produced}}$$

$$= \frac{\text{charge } (C) \text{ required to form Li (measured by mass of Li)}}{\text{total charge } (C) \text{ passed during chronopotentiometry}}$$

$$\times \frac{\text{measured production of } C_2H_2 \text{ (g)}}{\text{expected production of } C_2H_2 \text{ (g) if all Li reacted to form } Li_2C_2} \times 100$$

We calculated current efficiency using the baseline average of 88.5% current efficiency to electrochemically produce lithium, and then multiplied that by the ratio of the measured production of acetylene gas over the maximum possible gas production if all Li had reacted to form Li_2C_2 upon exposure to the carbon source. We refer to that yield multiplied by 100 as the "% yield" or "acetylene production from Li." Finally, due to the stoichiometric limitations addressed in Table 1 and the discussion we can also consider what percent of the maximum stoichiometric yield was obtained, assuming a given reaction mechanism from the table.

Pourbaix diagram calculations

Calculations for the Pourbaix diagram are analogous with our recent work on this Li cycling strategy for ammonia synthesis.[12] For Fig. 3, the carbon reference is bulk graphite, the lithium reference is bulk lithium in its most stable crystal structure (BCC), the oxygen reference is $H_2O_{(g)}$–H_2, and the hydrogen reference is the standard hydrogen electrode, in which H_2 gas is in equilibrium with protons and electrons. The slope of each line on the Pourbaix diagram is equal to the coefficient on the proton–electron pairs in the chemical reaction describing the formation of the corresponding species from the reference states normalized to the number of lithium atoms in the formula unit. For example, the slope of the lithium hydride line is equal to 1, and the slope of the line corresponding to lithium carbonate is equal to −3, as can be easily determined from the chemical equations describing their formation from the reference states:

$$Li_{(s)} + (H^+ + e^-) \rightarrow LiH$$

$$2Li_{(s)} + C_{(s)} + 3H_2O_{(l)} - 6(H^+ + e^-) \rightarrow Li_2CO_3$$

Explicitly, for each species, the slope is given by

$$\text{slope} = N_H - N_{Li^+} - 2N_O$$

The intercept for each line is the free energy of formation of the corresponding species under ambient conditions (300 K, 1 atm). Then enthalpy of formation of each species was taken from the NIST Chemistry Web Book.[19] The ΔS_f for each species was assumed to be dominated by the gas phase species in the reaction describing the formation of each species from the reference states. The entropy of the gas phase species were also found in the NIST Chemistry Web Book.[19] Explicitly, the intercept is given by:

$$\text{Intercept} = \Delta H_f^0 - T\Delta S_f^0 - (N_{Li^+})k_bT\ln([Li^+]) + (N_H)k_bT\ln(\text{pH})$$

C–C coupling barrier calculations

The barrier for the C–C coupling reaction was calculated using density functional theory (DFT) geometric relaxations and the nudged elastic band (NEB) method.[20] For all DFT calculations, ASE-espresso was used to run the calculations,[21] the plane wave cutoff was 500 eV, and the density wave cutoff was 5000 eV. The RPBE exchange correlation functional was used,[22] and a 4, 4, 4 Monkhorst–Pack *k*-point grid was used.[23] The convergence requirement was that the maximum force on any atom be less than 0.05 eV $Å^{-1}$. The unit cell was a cube with side length 10.44 Å, and there were 54 atoms of Li in the unit cell. To identify the final state, a geometric relaxation was performed with two carbons occupying the same octahedral site. To identify the initial state, a relaxation was performed with individual carbon atoms in neighboring octahedral sites, and a separate relaxation was performed with individual carbon atoms in non-neighboring octahedral sites. The latter configuration was found to be more stable, so it was used as the initial state for the NEB calculation.

Physical characterization

X-ray diffraction (XRD) was performed using a Philips PANalytical X'Pert Pro in parallel beam mode with Cu Kα radiation and 0.04 rad Soller slits. Prior to XRD scanning, samples for were pressed flat and sealed with Kapton (polyimide) tape against a glass slide backing in an Ar filled glove box. Gas chromatography was performed using a Thermofisher TRACE 1310 gas chromatograph equipped with a TGBOND-Q Plot column and a thermal conductivity detector in series with a flame ionization detector for product detection. Fourier transform infrared radiation (FTIR) spectroscopy was performed using a Nicolet IS-50 FTIR Advanced Spectrometer equipped with a Nicolet 2 m gas cell (ZnSe windows) connected to heated vapor and vacuum gas lines. Raman spectroscopy was conducted using a Horiba XploRA Confocal Raman. The Raman measurements were collected with an excitation laser at 432 nm, and a grating size of 1200 gr mm^{-1} in ambient air conditions.

Conflicts of interest

There are no conflicts of interest to declare.

Acknowledgements

This work was supported by a research grant (9455) from VILLUM FONDEN.

References

1 K. P. Kuhl, T. Hatsukade, E. R. Cave, D. N. Abram, J. Kibsgaard and T. F. Jaramillo, Electrocatalytic Conversion of Carbon Dioxide to Methane and Methanol on Transition Metal Surfaces, *J. Am. Chem. Soc.*, 2014, **136**(40), 14107–14113.

2 J. T. Feaster, C. Shi, E. R. Cave, T. Hatsukade, D. N. Abram, K. P. Kuhl, C. Hahn, J. K. Nørskov and T. F. Jaramillo, Understanding Selectivity for the Electrochemical Reduction of Carbon Dioxide to Formic Acid and Carbon

Monoxide on Metal Electrodes, *ACS Catal.*, 2017, 7(7), 4822–4827.

3 S. Nitopi, E. Bertheussen, S. B. Scott, X. Liu, A. K. Engstfeld, S. Horch, B. Seger, I. E. L. Stephens, K. Chan, C. Hahn, J. K. Nørskov, T. F. Jaramillo and I. Chorkendorff, Progress and Perspectives of Electrochemical CO_2 Reduction on Copper in Aqueous Electrolyte, *Chem. Rev.*, 2019, **119**(12), 7610–7672.

4 G. Psofogiannakis, A. St-Amant and M. Ternan, Methane Oxidation Mechanism on Pt(111): A Cluster Model DFT Study, *J. Phys. Chem. B*, 2006, **110**(48), 24593–24605.

5 J. H. Montoya, A. A. Peterson and J. K. Nørskov, Insights into C–C Coupling in CO_2 Electroreduction on Copper Electrodes, *ChemCatChem*, 2013, **5**(3), 737–742.

6 Y. Lum, B. Yue, P. Lobaccaro, A. T. Bell and J. W. Ager, Optimizing C–C Coupling on Oxide-Derived Copper Catalysts for Electrochemical CO_2 Reduction, *J. Phys. Chem. C*, 2017, **121**(26), 14191–14203.

7 Y. Hori, A. Murata and R. Takahashi, Formation of hydrocarbons in the electrochemical reduction of carbon dioxide at a copper electrode in aqueous solution, *J. Chem. Soc., Faraday Trans. 1*, 1989, **85**(8), 2309–2326.

8 D. Kim, C. S. Kley, Y. Li and P. Yang, Copper nanoparticle ensembles for selective electroreduction of CO_2 to C2–C3 products, *Proc. Natl. Acad. Sci. U. S. A.*, 2017, **114**(40), 10560–10565.

9 Z.-Q. Liang, T.-T. Zhuang, A. Seifitokaldani, J. Li, C.-W. Huang, C.-S. Tan, Y. Li, P. De Luna, C. T. Dinh, Y. Hu, Q. Xiao, P.-L. Hsieh, Y. Wang, F. Li, R. Quintero-Bermudez, Y. Zhou, P. Chen, Y. Pang, S.-C. Lo, L.-J. Chen, H. Tan, Z. Xu, S. Zhao, D. Sinton and E. H. Sargent, Copper-on-nitride enhances the stable electrosynthesis of multi-carbon products from CO_2, *Nat. Commun.*, 2018, **9**(1), 3828.

10 Acetylene, in *Ullmann's Encyclopedia of Industrial Chemistry*.

11 P. E. Halstead and A. E. Moore, 769 the thermal dissociation of calcium hydroxide, *J. Chem. Soc.*, 1957, 3873–3875.

12 J. M. McEnaney, A. R. Singh, J. A. Schwalbe, J. Kibsgaard, J. C. Lin, M. Cargnello, T. F. Jaramillo and J. K. Norskov, Ammonia synthesis from N_2 and H_2O using a lithium cycling electrification strategy at atmospheric pressure, *Energy Environ. Sci.*, 2017, **10**(7), 1621–1630.

13 N. Tian, Y. Gao, Y. Li, Z. Wang, X. Song and L. Chen, Li_2C_2, a High-Capacity Cathode Material for Lithium Ion Batteries, *Angew. Chem., Int. Ed.*, 2016, **55**(2), 644–648.

14 R. Schmitz, R. Müller, S. Krüger, R. W. Schmitz, S. Nowak, S. Passerini, M. Winter and C. Schreiner, Investigation of lithium carbide contamination in battery grade lithium metal, *J. Power Sources*, 2012, **217**, 98–101.

15 M. Drüe, M. Seyring, A. Kozlov, X. Song, R. Schmid-Fetzer and M. Rettenmayr, Thermodynamic stability of Li_2C_2 and LiC_6, *J. Alloys Compd.*, 2013, **575**, 403–407.

16 *HITRANonline*, accessed October 2018, http://hitran.org/.

17 M. Stoukides, Electrochemical studies of methane activation, *J. Appl. Electrochem.*, 1995, **25**(10), 899–912.

18 S. Konar, U. Häusserman and G. Svensson, Intercalation Compounds from LiH and Graphite: Relative Stability of Metastable Stages and Thermodynamic Stability of Dilute Stage Id, *Chem. Mater.*, 2015, **27**(7), 2566–2575.

19 D. R. Burgess, Thermochemical Data, in *NIST Chemistry WebBook, NIST Standard Reference Database Number 69*, ed. P. J. Linstrom and W. G. Mallard, National Institute of Standards and Technology, Gaithersburg MD, p. 20899, DOI: 10.18434/T4D303, retrieved February 4, 2019.

20 G. Henkelman, B. P. Uberuaga and H. Jónsson, Climbing image nudged elastic band method for finding saddle points and minimum energy paths, *J. Chem. Phys. A*, 2000, **113**, 9901.

21 S. R. Bahn and K. W. Jacobsen, An object-oriented scripting interface to a legacy electronic structure code, *Comput. Sci. Eng.*, 2002, **4**(3), 56–66.

22 B. Hammer, L. B. Hansen and J. K. Nørskov, Improved adsorption energetics within density functional theory using revised perdew-burke-ernzerhof functionals, *Phys. Rev. B: Condens. Matter Mater. Phys.*, 1999, **59**, 7413–7421.

23 H. J. Monkhorst and J. D. Pack, Special points for Brillouin-zone integrations, *Phys. Rev. B: Condens. Matter Mater. Phys.*, 1976, **13**, 5188–5192.